Journal of Power Sources 196 (2011) 10502–10506

Contents lists available at ScienceDirect

Journal of Power Sources

journal homepage: www.elsevier.com/locate/jpowsour

Short communication

Low-temperature synthesis of $Na_2Mn_5O_{10}$ for supercapacitor applications

Sheng Liu[a,b], Cheng-Zhi Fan[a,b], Yuan Zhang[a,b], Cheng-Hui Li[a,b,*], Xiao-Zeng You[a,b,*]

[a] State Key Laboratory of Coordination Chemistry, School of Chemistry and Chemical Engineering, Nanjing National Laboratory of Microstructures, Nanjing University, Nanjing 210093, PR China
[b] Academician Work Station of Changzhou Trina Solar Energy Co., Ltd., Changzhou 213022, Jiangsu Province, PR China

ARTICLE INFO

Article history:
Received 2 July 2011
Received in revised form 2 August 2011
Accepted 3 August 2011
Available online 10 August 2011

Keywords:
Supercapacitor
Sodium manganese oxide
Romanechite
Low temperature synthesis

ABSTRACT

The romanechite-like sodium manganese oxide $Na_2Mn_5O_{10}$ is synthesized through alkaline hydrolysis of $[Mn_{12}O_{12}(CH_3COO)_{16}(H_2O)_4]$ followed by thermal calcination. Amorphous $Na_2Mn_5O_{10}$ is obtained at relatively low temperature (200 °C). Increasing the calcination temperature leads to highly crystalline nano-rods. Electrochemical studies demonstrate that $Na_2Mn_5O_{10}$ is a good candidate as positive electrode materials for supercapacitor: specific capacitances of 178, 173 and 175 F g^{-1} are obtained for $Na_2Mn_5O_{10}$ calcined at different temperatures (200, 400 and 600 °C), respectively, by charge–discharge tests at 0.1 A g^{-1}. Moreover, capacitance losses of all the products in 1000 cycles are less than 3%.

1. Introduction

Electrochemical supercapacitors have attracted a lot of attention in power source applications due to their high power density, excellent reversibility and long cycle life [1]. High surface-area carbons, metal oxides, and conducting polymers are widely used as electrode materials in electrochemical supercapacitors. So far, amorphous $RuO_2{\cdot}xH_2O$ was reported as the most promising electrode material for supercapacitor with the highest specific capacitance. However, the high cost and environmental toxicity of this material limit its commercial application. Manganese oxides are promising replacements for RuO_2 as supercapacitor materials due to its good electrochemical performance, high specific capacitance, low cost, and environmental friendness [2,3]. Among the large quantity of manganese oxides reported in literatures, Li–Mn–O or Na–Mn–O systems have received extensive attention due to their tunnel or layered crystal structures which facilitate the lithium/sodium intercalation-deintercalation [4,5]. However, previous studies have mostly focused on the performance of lithium/sodium manganese oxides as positive electrode for lithium storage devices. Few reports are related to their application as electrode materials for supercapacitors [6–9].

The dodeca-nuclear mixed valence manganese oxo-clusters $[Mn_{12}O_{12}(RCOO)_{16}(H_2O)_x]$ [10] have been well known for decades as single-molecule magnets due to their large magnetic anisotropy and mixed valence state. This kind of molecules have a preformed oxo-manganese core containing a central $[Mn_4^{IV}O_4]$ cube surrounded by a non-planar ring of eight outer Mn^{III} ions that are bridged and connected to the cube via μ_3-O^{2-} ions. Therefore, they could be promising precursors for the preparation of mixed valence manganese oxides with novel topology. Recently, Folch et al. demonstrated that various manganese oxides with different compositions and morphologies can be obtained via low-temperature hydrothermal reactions using $[Mn_{12}O_{12}(C_2H_5COO)_{16}(H_2O)_3]$ as a precursor [11,12]. In this work, we synthesized the romanechite-like sodium manganese oxide $Na_2Mn_5O_{10}$ (also known as $Na_{0.4}MnO_2$) through alkaline hydrolysis of $[Mn_{12}O_{12}(CH_3COO)_{16}(H_2O)_4]$ followed by thermal calcination. The electrochemical capacitor performances of as-prepared $Na_2Mn_5O_{10}$ samples were also investigated.

2. Experimental

2.1. Materials

$[Mn_{12}O_{12}(CH_3COO)_{16}(H_2O)_4]$ was prepared according to the literature method [10]. In a typical synthesis of $Na_2Mn_5O_{10}$, 0.1 g (0.048 mmol) $[Mn_{12}O_{12}(CH_3COO)_{16}(H_2O)_4]$ was dissolved in 25 mL of C_2H_5OH, filtered and added to 25 mL of a saturated solution of NaOH in C_2H_5OH. The mixture was vigorously stirred for 2 h. The resulting dark brown participate was filtered, washed with H_2O,

* Corresponding authors at: State Key Laboratory of Coordination Chemistry, School of Chemistry and Chemical Engineering, Nanjing National Laboratory of Microstructures, Nanjing University, Nanjing 210093, PR China.
Tel.: +86 25 83592969; fax: +86 25 83314502.
E-mail addresses: chli@nju.edu.cn (C.-H. Li), youxz@nju.edu.cn (X.-Z. You).

0378-7753/$ – see front matter © 2011 Elsevier B.V. All rights reserved.
doi:10.1016/j.jpowsour.2011.08.014

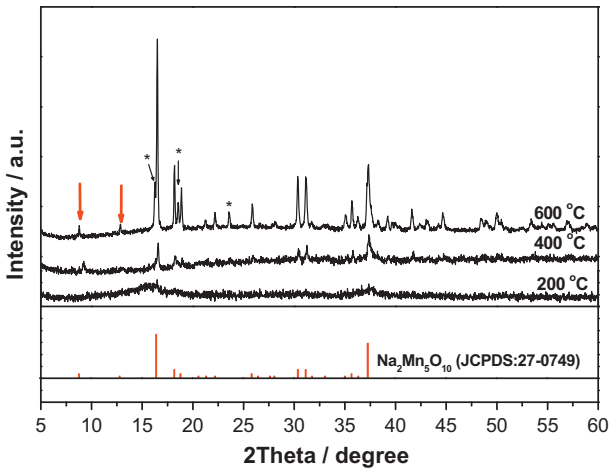

Fig. 1. X-ray powder diffraction pattern of $Na_2Mn_5O_{10}$ calcined at different temperatures.

C_2H_5OH, acetone, ether, and dried under vacuum. The resulting brown solid was ground into fine powder and then calcined at different temperatures (200, 400 and 600 °C, respectively) for 5 h. Yields: 90–95%.

2.2. Characterization of $Na_2Mn_5O_{10}$

The crystalline structure of the products was determined by a XRD-6000 powder diffractometer (Shimadzu, Japan) using Cu Kα radiation between 5° and 60° with a scanning rate of 2° min^{-1}. The morphologies of the samples were observed by a scanning electron microscope Model S-4800 (SEM, Hitachi, Japan). The Brunauer–Emmett–Teller (BET) surface areas were measured by using Micromeritics ASAP 2020 M + C volumetric adsorption equipment. The X-ray photoelectron spectroscopies (XPS) were investigated using a PHI 5000 VersaProbe X-ray photoelectron spectrometer.

2.3. Preparation of $Na_2Mn_5O_{10}$ electrodes

The electrodes were prepared by mixing 80 wt.% $Na_2Mn_5O_{10}$ powders, 15 wt.% acetylene black and 5 wt.% poly(tetrafluoroethylene) (PTFE) binder. Typical loading level of the active material masses on the current collector ranged from 10 to 15 mg cm^{-2} with the typical surface areas of 2–3 cm^2.

2.4. Electrochemical measurements of $Na_2Mn_5O_{10}$ electrodes

Electrochemical characterization of $Na_2Mn_5O_{10}$ electrodes were examined by means of a three-compartment cell using Pt foil as counter electrode and saturated Ag/AgCl as reference electrode at room temperature. The cyclic voltammetry and galvanostatic charge/discharge tests were performed by an electrochemical analyzer system, CHI 660D (CH Instruments). The ac impedance spectra were collected using Zahner Im6eX Electrochemical Workstation. An ac amplitude of 5 mV was applied to reach the steady-state cell voltage, and the data were collected in the range of 10,000–0.1 Hz.

3. Result and discussion

3.1. XRD analysis and morphology of $Na_2Mn_5O_{10}$

Fig. 1 shows the XRD patterns of the obtained $Na_2Mn_5O_{10}$. Only broad diffraction peaks were observed for the sample prepared at 200 °C, indicating the presence of an amorphous phase. The

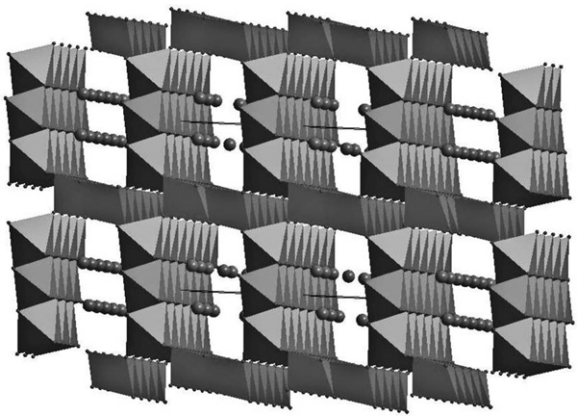

Fig. 2. Schematic diagram of the romanechite structure.

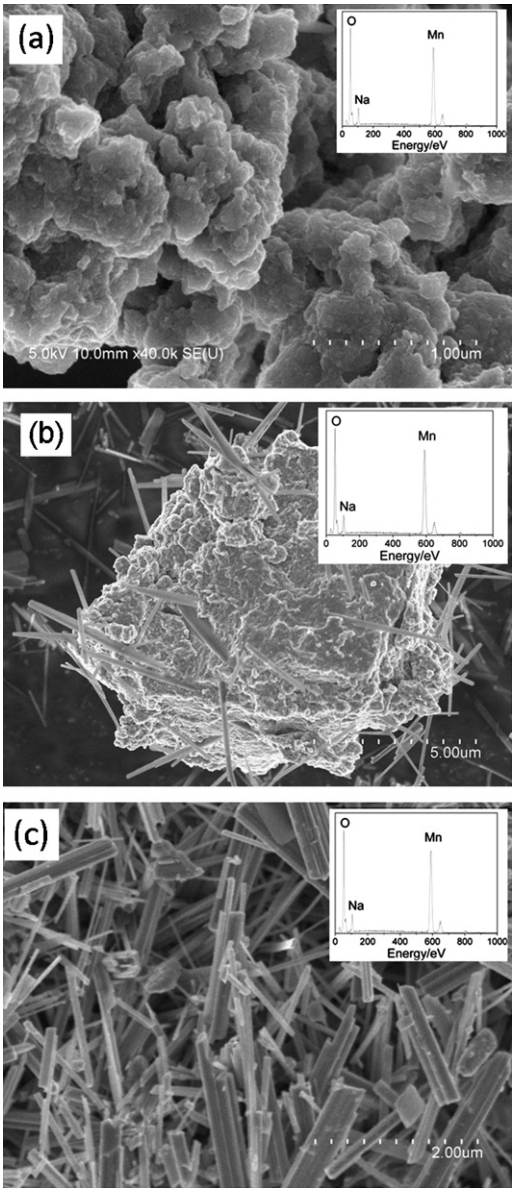

Fig. 3. SEM images of $Na_2Mn_5O_{10}$ calcined at different temperatures: (a) 200 °C; (b) 400 °C; (c) 600 °C. Insert: The energy dispersive X-ray spectrum of the $Na_2Mn_5O_{10}$ samples.

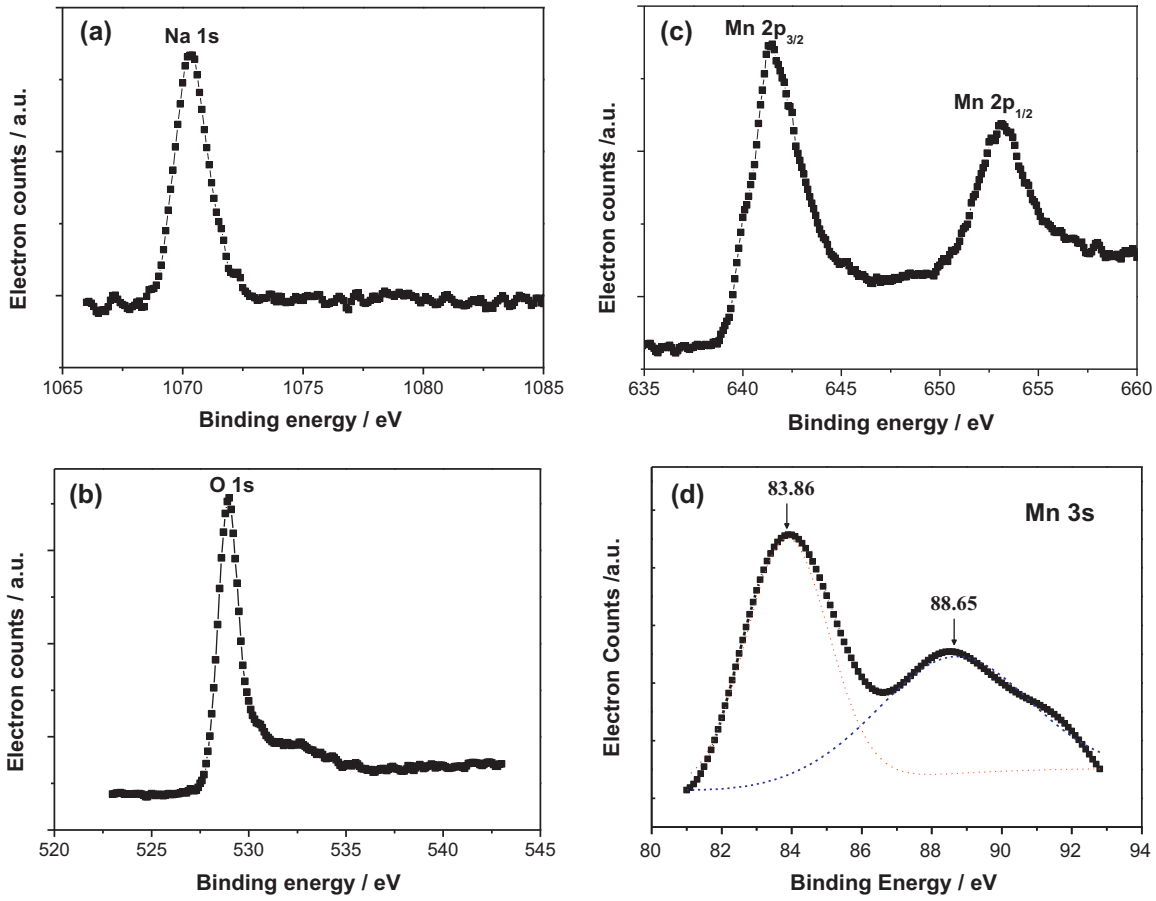

Fig. 4. XPS spectra for the $Na_2Mn_5O_{10}$ calcinated at 200 °C: (a) Na 1s; (b) O 1s; (c) Mn 2p; (d) Mn 3s.

crystallinity increases with increasing the calcination temperature. The structure of the product annealed at 600 °C can be identified as $Na_2Mn_5O_{10}$ (JCPDS 27–0749) [13]. Peculiar peaks of romanechite structure were observed at 8.8 and 12.8°, as indicated by arrows in Fig. 1. According to previous studies, $Na_2Mn_5O_{10}$ possesses a (2×3) tunnel structure which consists of MnO_6 octahedral units shared by corners and/or edges as shown in Fig. 2. Some additional peaks (marked by *) were observed, which cannot be definitely indexed to a specific phase according to JCPDS. Interestingly, these same peaks were also found in the work of both Hu et al. [14] and Tsuda et al. [15] on $Na_2Mn_5O_{10}$ synthesized by different methods.

Fig. 3 shows the SEM images of the synthesized $Na_2Mn_5O_{10}$. The sample obtained at 200 °C consists of homogeneous amorphous powders (Fig. 3(a)). With the annealing temperature increased to 400 °C, the amorphous powders begin to grow into the nanorods (Fig. 3(b)). Upon further heating to 600 °C, well-defined nanorods are observed (Fig. 3(c)). Energy dispersive X-ray (EDX) analysis reveals that all the samples contain Na, Mn, and O with Na/Mn/O ratio of 0.41:1:1.99, closed to 0.4:1:2 derived from the molecular formula. The BET specific surface areas of the samples calcined at different temperatures are calculated to be 9–11 $m^2\,g^{-1}$.

3.2. XPS study of $Na_2Mn_5O_{10}$

The $Na_2Mn_5O_{10}$ samples were also characterized by X-ray photoelectron spectroscopy (XPS) (Fig. 4). The Na 1s and O 1s peaks were observed at 1071 and 529 eV, respectively. The Mn $2p_{3/2}$ and Mn $2p_{1/2}$ are centered at 641.5 and 653.1 eV. The Mn 3s spectrum exhibits two peaks due to multiplet splitting. The separation of the two peaks is used to calculate the mean oxidation state of Mn in the products according to the works by Chigane and Ishikawa [16] and Gao et al. [17]. The peak separation in the Mn 3s spectrum is observed at 4.79 eV, corresponding to a mean oxidation state of 3.6, which is in agreement with that derived from the molecular formula.

The synthesis of $Na_2Mn_5O_{10}$ was rarely reported in the literature and generally produced with high-temperature solid state reaction [13–15]. Moreover, the presence of an analogue phase $Na_4Mn_9O_{18}$ (also known as $Na_{0.44}MnO_2$) with close composition but a different tunnel structure often makes it difficult to obtain pure materials of $Na_2Mn_5O_{10}$. Our work provides a new way to synthesize $Na_2Mn_5O_{10}$ at relatively low temperature.

3.3. Cyclic voltammetry

Fig. 5(a) shows the cyclic voltammogram of the $Na_2Mn_5O_{10}$ composite electrodes in aqueous 0.5 M Na_2SO_4 electrolyte at the scan rate of 2 $mV\,s^{-1}$. The cyclic voltammetry (CV) curves of amorphous sample shows an ideal rectangular shape without any noticeable redox peaks from 0 to 0.8 V. However, redox peaks were observed for crystalline samples. The highly reversible pairs of redox peaks are most apparent for the sample annealed at 600 °C. The shapes of cyclic voltammogram at high sweep rates differ from rectangular and the redox peaks disappeared (Fig. 5(b)).

Two mechanisms have been proposed to elucidate the charge storage behavior of manganese oxides in aqueous electrolytes [2,18,19], both of which share the same reaction formula as followed (M represents the hydrated protons or cations like Li^+, Na^+ and K^+):

$$MnO_2 + M^+ + e^- \leftrightharpoons MnOOM$$

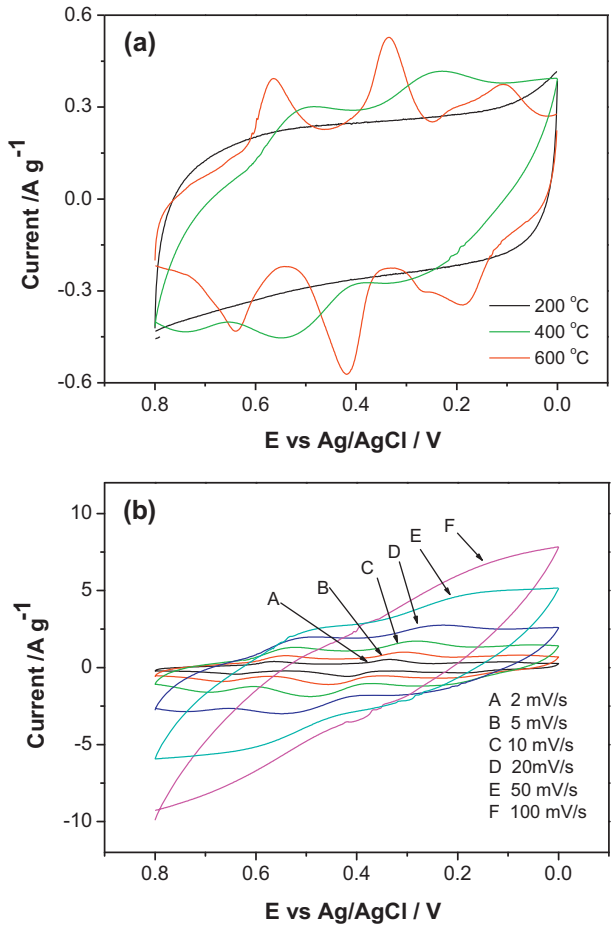

Fig. 5. (a) Cyclic voltammogram of $Na_2Mn_5O_{10}$ electrodes at the scan rate of 2 mV s^{-1}; (b) Variable scan rate cyclic voltammogram of $Na_2Mn_5O_{10}$ electrode calcined at 600 °C.

The first mechanism is an adsorption/desorption process of cations at the material surface, which occurs mostly in amorphous manganese oxides. The second mechanism, however, is an intercalation/deintercalation process of cations into the material bulk and is expected to be predominant in crystalline manganese oxides.

The differences in cyclic voltammograms of composite electrode based on $Na_2Mn_5O_{10}$ annealed at 200, 400 and 600 °C can thus be ascribed to the different mechanisms. The redox peaks in the CV curves of crystalline materials can be attributed to the repetitive Na^+ intercalation and deintercalation. Similar observations were found in the work of Ragupathy et al. [20].

3.4. Galvanostatic charge–discharge analysis

As seen in Fig. 6, the charge–discharge curve for amorphous $Na_2Mn_5O_{10}$ at 0.1 A g^{-1} is almost linear in the total range of potential with a constant slope, showing nearly perfect capacitive behavior. The crystalline electrodes show slight deviation from the linear line with some very short plateaus. This is in agreement with results from CV study (see above). The durations of charging and discharging are almost equal for each electrode, implying high columbic efficiency of charge/discharge cycling. The specific capacitance of the samples calcined at 200, 400, 600 °C are 178, 173 and 175 F g^{-1}, respectively. These values are slightly higher than those reported by Kuratani et al. [6], Athouel et al. [7] and Holze and co-workers [8] (140–145 F g^{-1}), but significantly lower than that of $Na_4Mn_9O_{18}$ (324 F g^{-1}) reported by Whitacre et al. [9]. The high specific capacitances of $Na_4Mn_9O_{18}$ may be attributed to the better ionic conductivity and larger BET surface area induced by its unusual double tunnel structure [21,22].

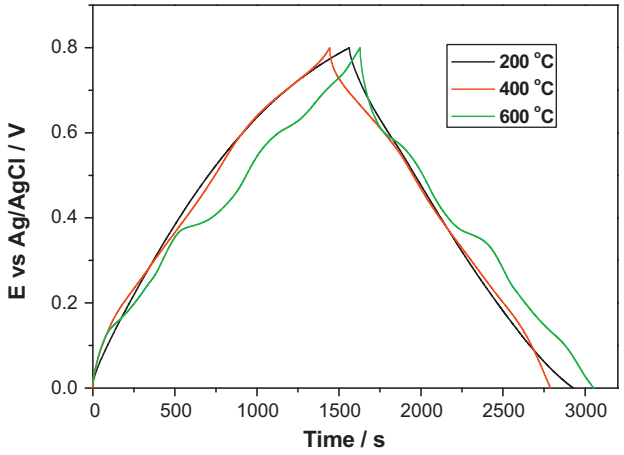

Fig. 6. Charge/discharge curves of $Na_2Mn_5O_{10}$ electrodes at constant current of 0.1 A g^{-1}.

The rate performances of the supercapacitor based on $Na_2Mn_5O_{10}$ were examined at various current rates ranging from 0.1 A g^{-1} to 1 A g^{-1} (Fig. 7). The specific capacitance at 1 A g^{-1} is about 70% of that in 0.1 A g^{-1}, indicating that the supercapacitor using $Na_2Mn_5O_{10}$ as the electrode material can undertake high current in practical applications. The cycle life of composite electrodes based on $Na_2Mn_5O_{10}$ was examined at a current density of 0.1 A g^{-1}. The variations of specific capacitance over 1000 cycles are depicted in Fig. 8. The capacitance losses of all the products after 1000 cycles of charge/discharge tests are less than 3%.

3.5. Ac impedance spectroscopy

The ac impedance plots of $Na_2Mn_5O_{10}$ composite electrodes at an applied potential of 0.2 V (vs Ag/AgCl) in 0.5 M Na_2SO_4 solutions are presented in Fig. 9. These impedance plots are characterized by two distinct parts, a semicircle at high-frequency and a linear line at low-frequency. An intercept at Z'-axis in the high frequency region identifies the bulk solution resistances (R_s), while the radius of the semicircle at high frequency region on the Z'-axis is related to the charge transfer resistance (R_{ct}). It is evident that the bulk solution resistances R_s are almost the same for all the samples. However, the charge transfer resistance (R_{ct}) decreases as the increase of calcination temperature.

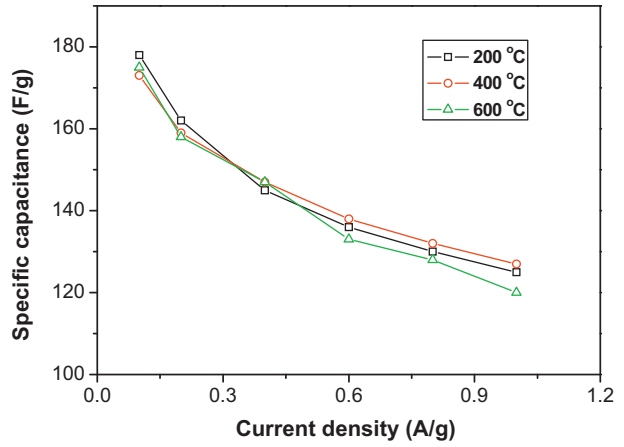

Fig. 7. The plot of specific capacitance versus discharge current density of $Na_2Mn_5O_{10}$ electrodes.

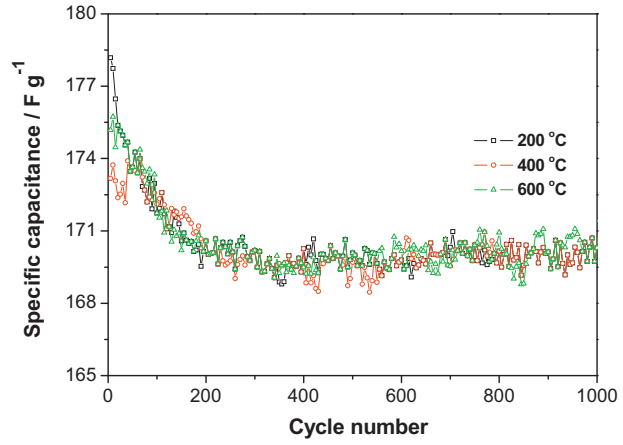

Fig. 8. Variation of the specific capacitance of $Na_2Mn_5O_{10}$ electrodes as a function of the number of cycles (0.1 A g^{-1}).

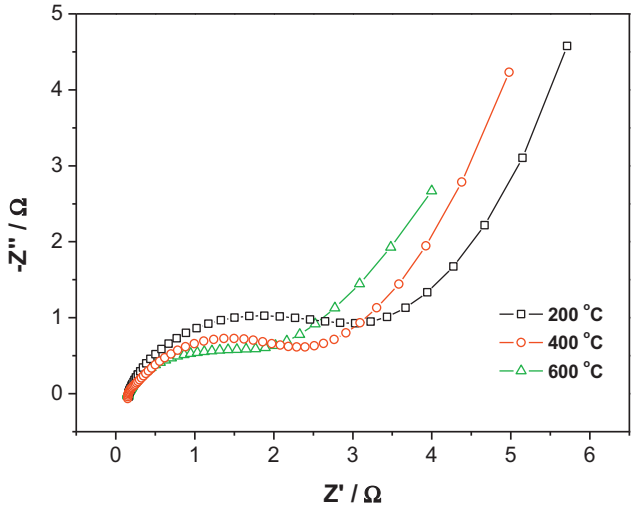

Fig. 9. The Ac impedance spectra of $Na_2Mn_5O_{10}$ electrodes at an applied potential of 0.2 V (vs Ag/AgCl).

4. Conclusion

We synthesized the romanechite-like sodium manganese oxide $Na_2Mn_5O_{10}$ through alkaline hydrolysis of $[Mn_{12}O_{12}(CH_3COO)_{16}(H_2O)_4]$ followed by thermal calcination. The amorphous sample was obtained at low temperature (200 °C), which can be converted into highly crystalline nano-rods upon calcination at high temperature (600 °C). Both the amorphous powder and high crystalline nano-rods show good performance as positive electrode materials for supercapacitors. More detailed electrochemical evaluations of the $Na_2Mn_5O_{10}$ as positive electrode materials are in progress, with the aim of obtaining porous $Na_2Mn_5O_{10}$ to increase the surface area of these electrodes in supercapacitors.

Acknowledgments

This work was supported by the National Basic Research Program of China (2007CB925100, 2011CB808704 and 2011CB933300), the National Natural Science Foundation of China (91022031, 21021062), and the funding from Academician Workstation in Changzhou Trina Solar Energy Co. Ltd., Jiangsu Province. We thank Prof. Yong Zhou, Dr. Ming-Bo Zheng and Dr. Huan Pang for their kind help and suggestions.

References

[1] B.E. Conway, Electrochemical Supercapacitors: Scientific Fundamentals and Technological Applications, Kluwer Academic/Plenum Publishers, New York, 1999.
[2] H.Y. Lee, J.B. Goodenough, Journal of Solid State Chemistry 144 (1999) 220–223.
[3] W. Wei, X. Cui, W. Chen, D.G. Ivey, Chemical Society Reviews 40 (2011) 1697–1721.
[4] Q. Feng, H. Kanoh, K. Ooi, Journal of Materials Chemistry 9 (1999) 319–333.
[5] S.L. Brock, N. Duan, Z.R. Tian, O. Giraldo, H. Zhou, S.L. Suib, Chemistry of Materials 10 (1998) 2619–2628.
[6] K. Kuratani, K. Tatsumi, N. Kuriyama, Crystal Growth and Design 7 (2007) 1375–1377.
[7] L. Athouel, F. Moser, R. Dugas, O. Crosnier, D. Belanger, T. Brousse, The Journal of Physical Chemistry C 112 (2008) 7270–7277.
[8] Q.T. Qu, Y. Shi, S. Tian, Y.H. Chen, Y.P. Wu, R. Holze, Journal of Power Sources 194 (2009) 1222–1225.
[9] J.F. Whitacre, A. Tevar, S. Sharma, Electrochemistry Communications 12 (2010) 463–466.
[10] R. Sessoli, H.L. Tsai, A.R. Schake, S. Wang, J.B. Vincent, K. Folting, D. Gatteschi, G. Christou, D.N. Hendrickson, Journal of the American Chemical Society 115 (1993) 1804–1816.
[11] B. Folch, J. Larionova, Y. Guari, C. Guerin, C. Reibel, Journal of Solid State Chemistry 178 (2005) 2368–2375.
[12] B. Folch, J. Larionova, Y. Guari, C. Guerin, A. Mehdi, C. Reye, Journal of Materials Chemistry 14 (2004) 2703–2711.
[13] J.P. Parant, R. Olazcuag, M. Devalett, C. Fouassie, P. Hagenmul, Journal of Solid State Chemistry 3 (1971) 1–11.
[14] F. Hu, M.M. Doeff, Journal of Power Sources 129 (2004) 296–302.
[15] M. Tsuda, H. Arai, Y. Nemoto, Y. Sakurai, Journal of the Electrochemical Society 150 (2003) A659–A664.
[16] M. Chigane, M. Ishikawa, Journal of the Electrochemical Society 147 (2000) 2246–2251.
[17] T. Gao, P. Norby, F. Krumeich, H. Okamoto, R. Nesper, H. Fjellvag, Journal of Physical Chemistry C 114 (2010) 922–928.
[18] V. Subramanian, H.W. Zhu, B.Q. Wei, Journal of Power Sources 159 (2006) 361–364.
[19] M. Toupin, T. Brousse, D. Bélanger, Chemistry of Materials 16 (2004) 3184–3190.
[20] P. Ragupathy, H.N. Vasan, N. Munichandraiah, Journal of the Electrochemical Society 155 (2008) A34–A40.
[21] J. Akimoto, H. Hayakawa, N. Kijima, J. Awaka, F. Funabiki, Solid State Phenomena 170 (2011) 198–202.
[22] O. Ghodbane, J.-L. Pascal, F. Favier, ACS Applied Materials and Interfaces 1 (2009) 1130–1139.